Virus Research 344 (2024) 199358

Contents lists available at ScienceDirect

Virus Research

journal homepage: www.elsevier.com/locate/virusres

An evolutionary theory on virus mutation in COVID-19

Liaofu Luo [a,*], Jun Lv [b,*]

[a] Faculty of Physical Science and Technology, Inner Mongolia University, 235 West College Road, Hohhot 010021, China
[b] College of Science, Inner Mongolia University of Technology, 49 Aymin Street, Hohhot 010051, China

ARTICLE INFO

Keywords:
COVID-19
Spike protein
Virus mutation
Evolutionary theory

ABSTRACT

With the rapid evolution of SARS-CoV-2, the emergence of new strains is an intriguing question. This paper presents an evolutionary theory to analyze the mutations of the virus and identify the conditions that lead to the generation of new strains. We represent the virus variants using a 4-letter sequence based on amino acid mutations on the spike protein and employ an *n*-distance algorithm to derive a variant phylogenetic tree. We show that the theoretically-derived tree aligns with experimental data on virus evolution. Additionally, we propose an A-X model, utilizing the set of existing mutation sites (A) and a set of randomly generated sites (X), to calculate the emergence of new strains. Our findings demonstrate that a sufficient number of random iterations can predict the generation of new macro-lineages when the number of sites in X is large enough. These results provide a crucial theoretical basis for understanding the evolution of SARS-CoV-2.

1. Introduction

The novel coronavirus, SARS-CoV-2, has been undergoing continuous mutations for over three years, resulting in the emergence of various variants such as alpha, beta, gamma, delta, and omicron. The intricate interplay among virus antigenicity, transmission dynamics, and virulence introduces unpredictable implications for the future trajectory and disease burden of COVID-19 (Carabelli et al., 2023; Markov et al., 2023; Cao et al., 2023; Mallapaty, 2022; Callaway, 2021; Wang et al., 2023). Recently, several authors have put forward novel methods to predict the evolution of the COVID-19 pandemic. A network-based inference approach has been recommended, particularly suitable for short- to mid-term predictions but deemed less reliable for long-term forecasts (Rahnsch et al., 2024). Given the pivotal role of spike protein mutations in the rapid evolution of SARS-CoV-2, deep learning methodologies have been proposed to forecast future protein sequences, leveraging Large Language Models (Ramachandran et al., 2024; Fowler et al., 2014; Elnaggar et al., 2022; Ferruz et al., 2022). The PandoGen algorithm has demonstrated the ability to train protein language models for pandemic protein forecasting tasks (Ramachandran et al., 2024). However, predicting the recombinant lineages of SARS-CoV-2 using PandoGen and ensuring the continuous incorporation of new experimental data remain critical challenges for the algorithm.

Recent research has identified two primary forces controlling virus evolution: intrinsic transmissibility, determined by the ACE2 binding affinity of SARS-CoV-2, and immune evasion, achieved through a reduction in susceptibility to neutralizing antibodies (Ma et al., 2023). Based upon the aforementioned two forces we can design an evolutionary model on virus mutation. In a prior study (Luo and Lv, 2023), we introduced a mathematical model for analyzing the dynamics of COVID-19 spread, with a specific focus on the competitive dissemination of two viruses within a given region. Building upon this work, the present article puts forth an evolutionary theory concerning virus mutation in the context of COVID-19. Our approach involves deducing an evolutionary tree based on sound assumptions regarding mutant representation, alongside the application of a well-established tree construction algorithm. Importantly, we illustrate that the theoretical tree effectively mirrors the observed evolutionary patterns of existing virus strains. Moreover, leveraging a statistical method developed in our study, we extend the utility of the evolutionary tree to predict the emergence of novel macro-lineages of viruses. These findings supply a critical theoretical framework for comprehending the evolution of SARS-CoV-2.

2. Material and method

2.1. SARS-CoV-2 variants

We obtained a total of 25 variants from the mutation reports provided by outbreak.info (https://outbreak.info/, accessed on 15 October

* Corresponding authors.
E-mail addresses: lolfcm@imu.edu.cn (L. Luo), lujun@imut.edu.cn (J. Lv).

https://doi.org/10.1016/j.virusres.2024.199358
Received 15 November 2023; Received in revised form 16 March 2024; Accepted 17 March 2024

2023) (Gangavarapu et al., 2023). These variants belong to the SARS-CoV-2 Pango lineages. Our analysis focused solely on mutations that occurred in the spike protein of the virus. Additionally, we only included mutations that were found in at least 75 % of the sequenced SARS-CoV-2 lineages. Table 1 provides a comprehensive list of all 25 variants and their corresponding mutation sites.

2.2. ACE2 binding affinity of a single mutation

We obtained the data for single-point mutations affecting the interaction between the receptor-binding domain (RBD) (amino acid residues 331 to 531 on the spike protein) and the ACE2 receptor from reference (Starr et al., 2020). The mean and standard deviation of the affinity for the 19 mutations occurring at the i th residue are denoted as b_i and s_i, respectively. If the affinity value m_i for the i th residue is greater than b_i+s_i, the mutation is classified as an affinity-enhancing type. If $m_i<b_i-s_i$, the mutation is classified as an affinity-weakening type. If $b_i-s_i \le m_i \le b_i+s_i$, the mutation is considered to have little effect on the binding affinity.

2.3. The n-distance between two sequences

The evolutionary tree provides a detailed description of the relationships between different viral strains. Consistency with the tree of life is a stringent requirement for any proposed evolutionary model, making it a sensitive test for such models. Let p_a represent the probability of a letter "a" (where a can be 0, 1, 2, or 3) occurring in a sequence, and let p_{ab} represent the joint probability of letters "a" and "b" appearing sequentially in the sequence. In general, let $\sigma=abc\ldots$ represent an n-letter segment, and let p_σ denote the joint probabilities of the bases in σ occurring in the sequence. In the calculation of joint probabilities, all sequences are assumed to be circular. For any given n, the sum of the joint probabilities over all segments σ of length n is always equal to 1. This can be written as $\sum\limits_\sigma p_\sigma = 1$, where the summation is over the set of all 4^n segments of length n. Given two sequences Σ and Σ' with sets of joint probabilities $\{p_\sigma\}$ and $\{p'_\sigma\}$ respectively, we define a distance, called an n-distance, between the two sequences based on the difference in joint probabilities as follows:

$$E_n(\Sigma, \Sigma') = \sum_\sigma |p_\sigma - p'_\sigma|, n = 1, 2, \ldots. \tag{1}$$

In the following, when there is no confusion, the arguments of E_n will be omitted. An n-distance is well-defined for sequences of different lengths that are not aligned. By repeatedly applying relations such as Eq. (2) below:

$$|p_\sigma - p'_\sigma| = \left|\sum_a (p_{\sigma a} - p'_{\sigma a})\right| \le \sum_a |p_{\sigma a} - p'_{\sigma a}|, \tag{2}$$

where σ is any n-letter segment and σa is an $(n+1)$-letter segment, it can be deduced that:

$$E_{n+1} \ge E_n, n = 1, 2, \ldots. \tag{3}$$

2.4. The construction method of the evolutionary tree

To infer the phylogenetic tree, three main algorithms are commonly used in the literature, based on the evolutionary information contained in the sequences: distance matrix treeing, maximum parsimony analysis, and maximum likelihood method (Li, 1997). In the distance matrix method, evolutionary distances are initially computed for all pairs of taxa. Subsequently, a phylogenetic tree is constructed using an algorithm (such as the unweighted pair-group method with arithmetic mean or UPGMA, the neighbor-joining method or NJ, etc.) that relies on functional relationships among the distance values. The maximum likelihood method involves studying the relationship between each

Table 1
Mutated sites on spike protein of 25 selected SARS-CoV-2 mutants.

macro-lineage	variant	number of mutated sites	mutated sites[1]
N-lineage	Alpha	10	69, 70, 144, **501**, 570, 614, 681, 716, 982, 1118
	Beta	10	80, 215, 241, 242, 243, **417, 484, 501**, 614, 701
	Gamma	12	18, 20, 26, 138, 190, **417, 484, 501**, 614, 655, 1027, 1176
	Delta	9	19, 156, 157, 158, **452, 478**, 614, 681, 950
	Epsilon	4	13, 152, **452**, 614
	Zeta	3	**484**, 614, 1176
	Eta	9	52, 67, 69, 70, 144, **484**, 614, 677, 888
	Theta	7	**484, 501**, 614, 681, 1092, 1101, 1176
	Iota	4	5, 95, 253, 614
	Kappa	5	**452, 484**, 614, 681, 1071
	Lambda	14	75, 76, 246, 247, 248, 249, 250, 251, 252, 253, **452, 490**, 614, 859
	Mu	9	95, 144, 145, **346, 484, 501**, 614, 681, 950
O-lineage	BA.1	33	67, 69, 70, 95, 142, 143, 144, 145, 211, 212, **339, 371, 373, 375, 477, 478, 484, 493, 496, 498, 501, 505**, 547, 614, 655, 679, 681, 764, 796, 856, 954, 969, 981
	BA.2	31	19, 24, 25, 26, 27, 142, 213, **339, 371, 373, 375, 376, 405, 408, 417, 440, 477, 478, 484, 493, 498, 501, 505**, 614, 655, 679, 681, 764, 796, 954, 969
	BA.2.12.1	33	19, 24, 25, 26, 27, 142, 213, **339, 371, 373, 375, 376, 405, 408, 417, 440, 452, 477, 478, 484, 493, 498, 501, 505**, 614, 655, 679, 681, 704, 764, 796, 954, 969
	BA.2.75	30	19, 24, 210, 213, 257, **339, 371, 373, 375, 376, 405, 408, 417, 440, 446, 460, 477, 478, 484, 498, 501, 505**, 614, 655, 679, 681, 764, 796, 954, 969
	BA.4.1	35	3, 19, 24, 25, 26, 27, 69, 70, 142, 213, **339, 371, 373, 375, 376, 405, 408, 417, 440, 452, 477, 478, 484, 486, 498, 501, 505**, 614, 655, 679, 681, 764, 796, 954, 969
	BA.5	34	19, 24, 25, 26, 27, 69, 70, 142, 213, **339, 371, 373, 375, 376, 405, 408, 417, 440, 452, 477, 478, 484, 486, 498, 501, 505**, 614, 655, 679, 681, 764, 796, 954, 969
	BF.7	35	19, 24, 25, 26, 27, 69, 70, 142, 213, **339, 346, 371, 373, 375, 376, 405, 408, 417, 440, 452, 477, 478, 484, 486, 498, 501, 505**, 614, 655, 679, 681, 764, 796, 954, 969
	BQ.1.1	37	19, 24, 25, 26, 27, 69, 70, 142, 213, **339, 346, 371, 373, 375, 376, 405, 408, 417, 440, 444, 452, 460, 477, 478, 484, 486, 498, 501, 505**, 614, 655, 679, 681, 764, 796, 954, 969
	CH.1.1	41	19, 24, 25, 26, 27, 142, 147, 152, 157, 210, 213, 257, **339, 346, 371, 373, 375, 376, 405, 408, 417, 440, 444, 446, 452, 460, 477, 478, 484, 486, 498, 501, 505**, 614, 655, 679, 681, 764, 796, 954, 969
	XBB.1.5	42	19, 24, 25, 26, 27, 83, 142, 144, 146, 183, 213, 252, **339, 346, 368, 371, 373, 375, 376, 405, 408, 417, 440, 445, 446, 460, 477, 478, 484, 486, 490, 498, 501, 505**, 614, 655, 679, 681, 764, 796, 954, 969

(*continued on next page*)

Table 1 (*continued*)

macro-lineage	variant	number of mutated sites	mutated sites[1]
	XBB.1.16	43	19, 24, 25, 26, 27, 83, 142, 144, 146, 180, 183, 213, 252, **339, 346, 368, 371, 373, 375, 376, 405, 408, 417, 440, 445, 446, 460, 477, 478, 484, 486, 490, 498, 501, 505**, 614, 655, 679, 681, 764, 796, 954, 969
	EG.1	37	19, 24, 25, 26, 27, 83, 142, 144, 146, 183, 213, 252, **339, 346, 368, 371, 373, 375, 376, 405, 408, 417, 440, 445, 446, 460, 477, 478, 484, 486, 490, 498, 501, 505**, 613, 614, 655
	EG.5.1	44	19, 24, 25, 26, 27, 52, 83, 142, 144, 146, 183, 213, 252, **339, 346, 368, 371, 373, 375, 376, 405, 408, 417, 440, 445, 446, 456, 460, 477, 478, 484, 486, 490, 498, 501, 505**, 614, 655, 679, 681, 764, 796, 954, 969
total	25 variants	104 mutation sits	3, 5, 13, 18, 19, 20, 24, 25, 26, 27, 52, 67, 69, 70, 75, 76, 80, 83, 95, 138, 142, 143, 144, 145, 146, 147, 152, 156, 157, 158, 180, 183, 190, 210, 211, 212, 213, 215, 241, 242, 243, 246, 247, 248, 249, 250, 251, 252, 253, 257, **339, 346, 368, 371, 373, 375, 376, 405, 408, 417, 440, 444, 445, 446, 452, 456, 460, 477, 478, 484, 486, 490, 493, 496, 498, 501, 505**, 547, 570, 613, 614, 655, 677, 679, 681, 701, 704, 716, 764, 796, 856, 859, 888, 950, 954, 969, 981, 982, 1027, 1071, 1092, 1101, 1118, 1176

[1] Mutated sites are considered when they occur in at least 75 % of the SARS—CoV-2 lineage sequences. Mutations in the receptor-binding domain (RBD) of the spike protein are indicated in bold.

sequence and the common ancestor in all possible trees. In this article, we utilized the UPGMA (Nei and Kumar, 2000) distance matrix method for constructing the phylogenetic tree. We attempted to use alternative algorithms to reconstruct the evolutionary tree of 25 virus strains but found that the UPGMA tree was superior to others (such as the NJ tree, etc.).

3. Results

3.1. Four-letter representation of the mutants

The surfaces of coronaviruses are decorated with a spike protein, about 1273 amino acids for SARS-COV-2. We propose representing any SARS-CoV-2 virus strain by a 1273-long sequence of four letters: 0, 1, 2, and 3. Here, 0 represents no mutation relative to the wild type, 1 represents a mutation having little effect on the ACE2 binding affinity, 2 represents a mutation of affinity-enhancing type, and 3 represents a mutation of affinity-weakening type.

We categorize the old SARS-CoV-2 mutants (alpha, beta, gamma, delta, etc.) as the N-lineage, while the recent mutants (omicron BA.2, BA.5, etc.) are classified as the O-lineage. We consider 12 main mutants in the N-lineage and 13 mutants in the O-lineage. Fig. 1 presents the representation of 25 mutants in the receptor-binding domain (RBD) of the spike protein, from site 331 to site 531. For example, the RBD of the Delta mutant is represented by (0,0,0,0,0,0,0,0,0,0,0,0,0,0,0,1,0,0,0,2,0,0,0,0,0,0,0), and the RBD of the BA.1 mutant is represented by (2,0,0,1,1,3,0,0,0,0,0,0,0,0,0,0,0,1,2,1,0,0,1,2,1,1,2). The sequences are 27 long, corresponding to 27 mutated sites. When considering all conservative sites denoted by 0 and inserting them in the sequence, we obtain 201-long sequences to describe the RBD. The 27-long sequence is the reduced sequence of the 201-long sequence.

The above representation for the RBD domain (201 sites) can be generalized to the full spike protein (1273 sites). Outside the RBD (sites 1 to 330 and sites 532 to 1273), only two letters, 0 and 1, occur since ACE2 binding does not occur in these domains. Thus, the full-spike representation of a SARS-CoV-2 mutant is a 1273-long sequence of four letters. Among the twenty-five known mutants, there are 104 mutated sites. Therefore, the reduced sequence of the full spike protein is a 104-long sequence. Table 1 lists the 25 selected mutants and their 104 mutated sites on the spike protein.

3.2. Evolutionary tree of virus mutation deduced by UPGMA method

Using the n-distance, we can construct a distance matrix D for a set of mutants labeled by $i, j, k, \ldots$, where the matrix element D_{ij} is equal to the n-distance between Σ_i and Σ_j, with Σ_i being the sequence representing mutant i. Then, by applying the UPGMA algorithm, we reconstruct the evolutionary tree of 25 mutants for a given value of n. We observed that the structure of the tree changes with increasing n and becomes stable after a few steps. Partial results are shown in Fig. 2. Specifically, when $n \geq 5$, the tree topology of the branch corresponding to macro-lineage O achieves stability. However, the structure of branch N slightly adjusts with increasing n. When $n \geq 7$, both branches O and N achieve stability as given in Fig. 2C.

Fig. 2C presents a UPGMA tree of 25 virus strains, displaying two distinct large branches corresponding to the macro-lineages N and O of existing virus strains. Notably, in macro-lineage O, the sub-branch accurately reflects the bifurcation of the earliest BA.1 strain and the subsequent BA.2, BA.4, BA.5 strains, as well as the correct classification of XBB as a recombination of two BA.2 strains. In macro-lineage N, the sub-branch of the tree shows four VOCs (variants of concern) - alpha, beta, delta, and gamma, belonging to independent sub-lineages. These observations highlight the highly consistent nature of the theoretical tree with all the evolutionary peculiarities of existing virus strains. This work presents a logically simple theory of virus mutation, whereby the tree is deduced from a single basic assumption - the four-letter representation of mutants and the n-distance algorithm for tree reconstruction. It is surprising that the theory aligns so well with experimental data.

The four-letter representation involves choosing between 0 and 1 for 104 mutational sites on the spike protein, while allowing for additional choices (i.e., choices 2 and 3 in addition to 0 and 1) for 27 sites on the RBD. The first part provides 104 bits of information, while the second part contributes only $\log(27\times19)/\log2=9$ bits of information. Therefore, to simplify calculations, one can approximate the four-letter representation as a two-letter representation that neglects choices 2 and 3. The validity of this approximation can be seen from the fact that the tree topology in Fig. 2 remains unchanged when the two-letter approximation is used.

3.3. Generation of new strain on the tree by stochastic method

Once the evolutionary tree is reconstructed based on known lineages of virus mutants, the generation of new strains on the tree can be examined. In this section, we propose a stochastic approach to address this problem. Let A be the set of all mutated sites in the updated virus strains, with the symbol a representing the number of sites. Each strain is represented by a two-letter sequence from the set A(a). Considering stochastic mutation on the spike protein, we define the set X (including x sites) as the set of sites participating in the stochastic sampling. The union of sets A(a) and X(x) is denoted as Z, with $Z = A\cup X$. The intersection of sets A and X is denoted as Y, which contains y sites and is represented as Y(y). Assuming that the new strain is generated by stochastic sampling in set Z, we discuss the new strain represented by a two-letter sequence from the union set Z(len), where $len=a + x\text{-}y$. Since the UPGMA tree provides a good description of the evolutionary

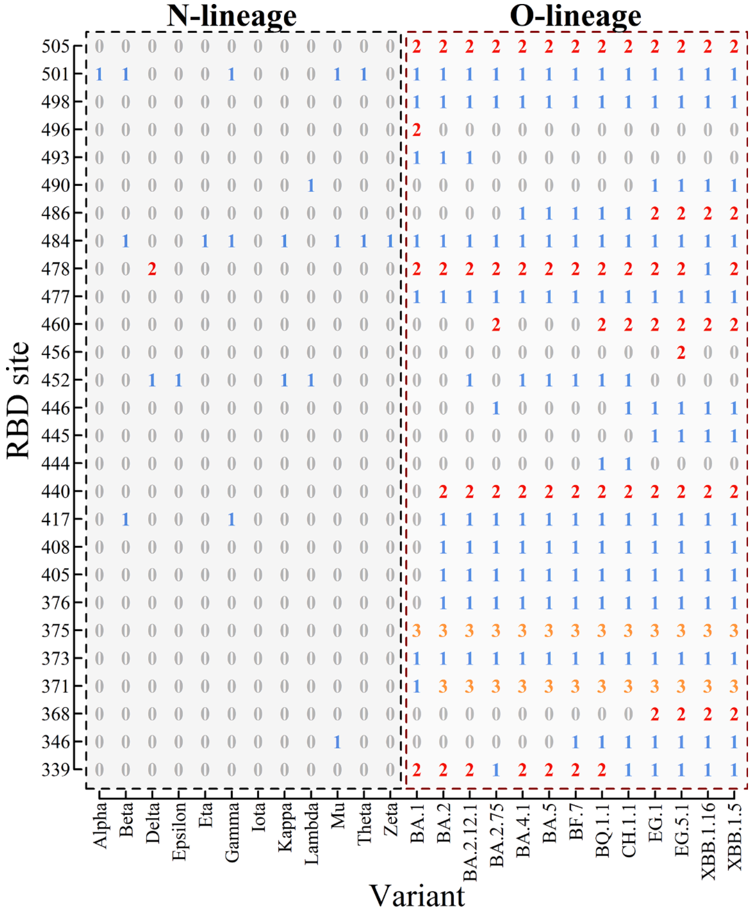

RBD site	Alpha	Beta	Delta	Epsilon	Eta	Gamma	Iota	Kappa	Lambda	Mu	Theta	Zeta	BA.1	BA.2	BA.2.12.1	BA.2.75	BA.4.1	BA.5	BF.7	BQ.1.1	CH.1.1	EG.1	EG.5.1	XBB.1.16	XBB.1.5
505	0	0	0	0	0	0	0	0	0	0	0	0	2	2	2	2	2	2	2	2	2	2	2	2	2
501	1	1	0	0	0	1	0	0	0	1	1	0	1	1	1	1	1	1	1	1	1	1	1	1	1
498	0	0	0	0	0	0	0	0	0	0	0	0	1	1	1	1	1	1	1	1	1	1	1	1	1
496	0	0	0	0	0	0	0	0	0	0	0	0	2	0	0	0	0	0	0	0	0	0	0	0	0
493	0	0	0	0	0	0	0	0	0	0	0	0	1	1	1	0	0	0	0	0	0	0	0	0	0
490	0	0	0	0	0	0	0	0	1	0	0	0	0	0	0	0	0	0	0	0	0	1	1	1	1
486	0	0	0	0	0	0	0	0	0	0	0	0	0	0	0	0	1	1	1	1	1	2	2	2	2
484	0	1	0	0	1	1	0	1	0	1	1	1	1	1	1	1	1	1	1	1	1	1	1	1	1
478	0	0	2	0	0	0	0	0	0	0	0	0	2	2	2	2	2	2	2	2	2	2	2	1	2
477	0	0	0	0	0	0	0	0	0	0	0	0	1	1	1	1	1	1	1	1	1	1	1	1	1
460	0	0	0	0	0	0	0	0	0	0	0	0	0	0	0	2	0	0	0	2	2	2	2	2	2
456	0	0	0	0	0	0	0	0	0	0	0	0	0	0	0	0	0	0	0	0	0	0	2	0	0
452	0	0	1	1	0	0	0	1	1	0	0	0	0	0	1	0	1	1	1	1	1	0	0	0	0
446	0	0	0	0	0	0	0	0	0	0	0	0	0	0	0	1	0	0	0	0	1	1	1	1	1
445	0	0	0	0	0	0	0	0	0	0	0	0	0	0	0	0	0	0	0	0	0	1	1	1	1
444	0	0	0	0	0	0	0	0	0	0	0	0	0	0	0	0	0	0	0	1	1	0	0	0	0
440	0	0	0	0	0	0	0	0	0	0	0	0	0	2	2	2	2	2	2	2	2	2	2	2	2
417	0	1	0	0	0	1	0	0	0	0	0	0	0	1	1	1	1	1	1	1	1	1	1	1	1
408	0	0	0	0	0	0	0	0	0	0	0	0	0	1	1	1	1	1	1	1	1	1	1	1	1
405	0	0	0	0	0	0	0	0	0	0	0	0	0	1	1	1	1	1	1	1	1	1	1	1	1
376	0	0	0	0	0	0	0	0	0	0	0	0	0	1	1	1	1	1	1	1	1	1	1	1	1
375	0	0	0	0	0	0	0	0	0	0	0	0	3	3	3	3	3	3	3	3	3	3	3	3	3
373	0	0	0	0	0	0	0	0	0	0	0	0	1	1	1	1	1	1	1	1	1	1	1	1	1
371	0	0	0	0	0	0	0	0	0	0	0	0	1	3	3	3	3	3	3	3	3	3	3	3	3
368	0	0	0	0	0	0	0	0	0	0	0	0	0	0	0	0	0	0	0	0	0	2	2	2	2
346	0	0	0	0	0	0	0	0	0	1	0	0	0	0	0	0	0	0	1	1	1	1	1	1	1
339	0	0	0	0	0	0	0	0	0	0	0	0	2	2	2	1	2	2	2	2	1	1	1	1	1

Fig. 1. Four-letter representation of mutant strains in the RBD. From the scale of the coordinate one can find 27 mutated sites on RBD from site 331 to 531 (referring to Table 1). The 4-letter representation of each strain is given in the column of the table.

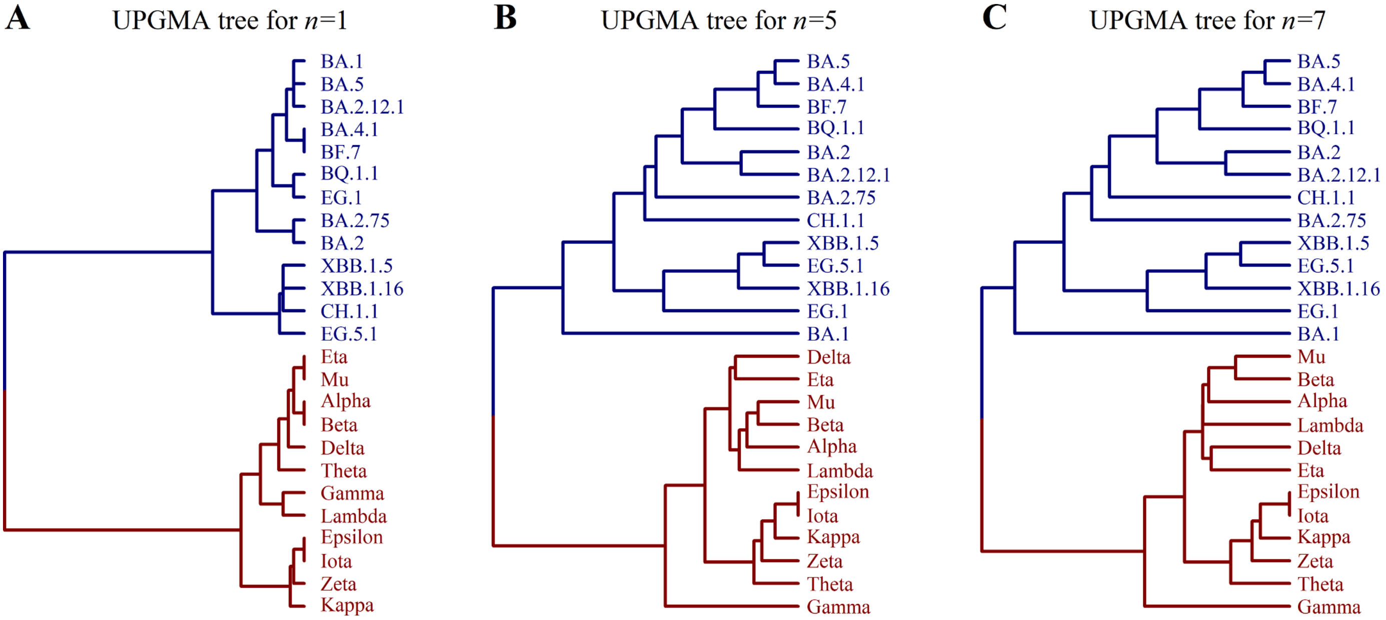

Fig. 2. Evolutionary tree describing virus mutation.

peculiarities of virus mutation, we use the UPGMA method (for $n = 7$) to reconstruct the evolutionary tree of the 25+1 mutants, where the additional strain is the predicted new strain. This approach is referred to as the A-X model.

In the A-X model, the new strain is represented by a two-letter sequence in the union set Z. Fig. 3A illustrates the schematic representation of the union set $Z = A \cup X$ and its relationship with sets A, X, and Y. Fig. 3B presents the coding rules for the 25 mutants and 1 new strain.

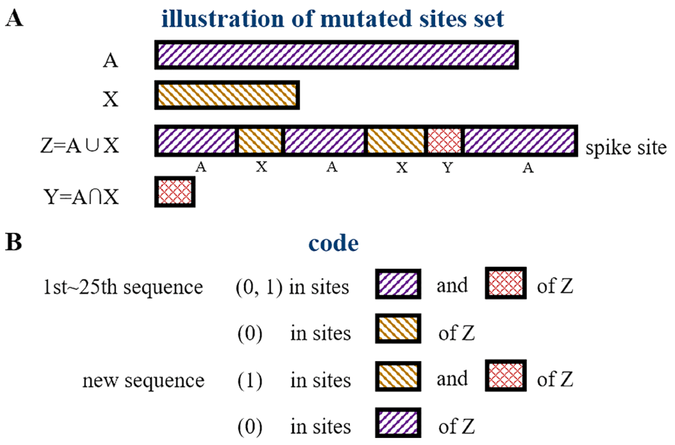
A
illustration of mutated sites set
A
X
Z=A∪X
spike site
A X A X Y A
Y=A∩X
B
code
1st~25th sequence (0, 1) in sites ▨ and ▦ of Z
(0) in sites ▨ of Z
new sequence (1) in sites ▨ and ▦ of Z
(0) in sites ▨ of Z

Fig. 3. Sketch map of mutated-site sets and coding rules.

Notice that no matter how the sets A and X are grouped along the sequence and how the set Y is inserted the new strain can always be predicted. The model ensures the correct prediction in case of continuous incorporation of new experimental data.

Now we aim to demonstrate the feasibility of the A-X model in predicting new strains of SARS-CoV-2.

By performing stochastic sampling $M = 10^5$ times, we obtained 10^5 predictions of new strains. Interestingly, when x is smaller than about 20, the predicted new strain always falls within one of the two major branches, N and O, as shown in Fig. 2. This indicates that the new strain belongs to either macro-lineage N or O. However, when x is large enough, an anomaly occurs, suggesting that the new strain may occur outside the branches N and O. In other words, the new strain does not belong to either lineage N or O for large values of M. We designate this new macro-lineage as P. Based on a typical stochastic sampling the generation of the new strain within the tree is illustrated in Fig. 4. For a given pair x and y the predicted new strain is represented as New$x.y$. In Fig. 4A, $x = 16$ and $y = 4$, the new strain is located within macro-lineage N; in Fig. 4B, $x = 16$ and $y = 1$, the new strain is located within macro-lineage O; in Fig. 4C, $x = 35$ and $y = 2$, the new strain is located within macro-lineage O; and in Fig. 4D, $x = 35$ and $y = 3$, the new strain is located within macro-lineage P. Therefore, the new strain can be predicted successfully through only two parameters x and y. This is the advantage of the A-X model.

3.4. The stochastic property of the intersection set

Since $M = 100{,}000$ corresponds to 16.6 bits of information, which is only 1.3 % of the 1273 bits for the entire spike protein, we employ a supplementary method to expand the range of stochastic sampling by randomizing the parameter y. This means that both the intersection set Y (y) and the union set Z($a + x$-y) are altered. In Fig. 4, we discovered that the change in the parameter y for a given x significantly affects the tree topology. Therefore, randomizing the parameter y is expected to be an efficient approach to enhance the stochastic information. To gain further insights into y-randomization, we performed six randomizations and

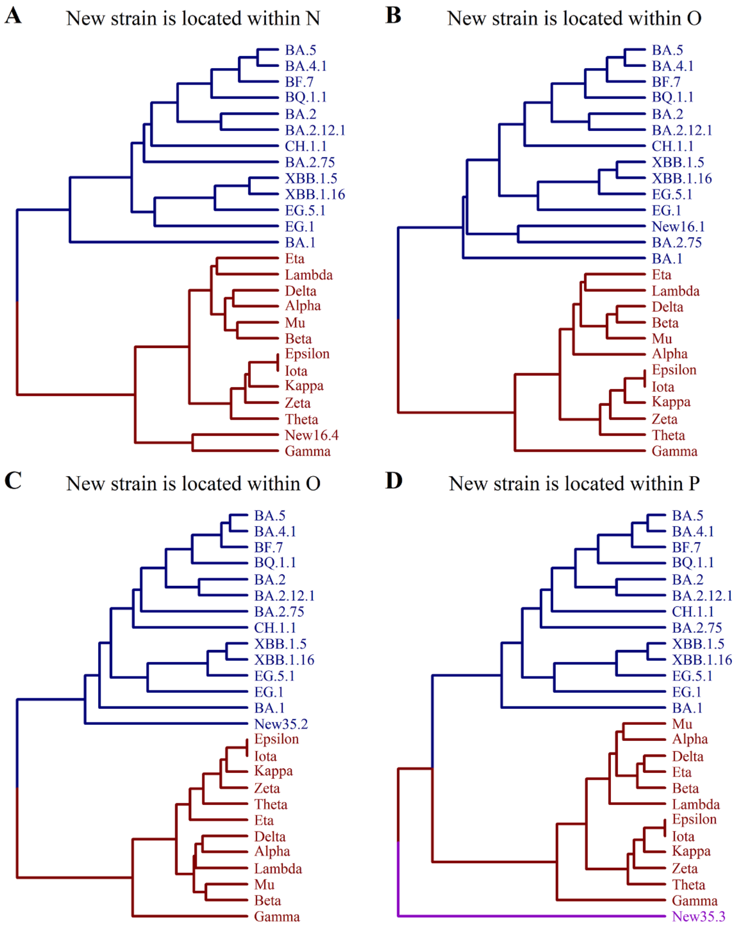

Fig. 4. Generation of new strain on the tree by use of the A-X model. The UPGMA tree for $n = 7$: (A) $x = 16$, $y = 4$; (B) $x = 16$, $y = 1$; (C) $x = 35$, $y = 2$; (D) $x = 35$, $y = 3$.

Table 2
Statistical distribution of y in six-times randomization.

x	distribution of y[1]					
	mean	sd	median	max	skew	kurtosis
13	1.06	0.98	1	7	0.84	0.54
13	1.06	0.98	1	7	0.84	0.55
13	1.06	0.98	1	7	0.83	0.52
13	1.06	0.98	1	7	0.82	0.46
13	1.06	0.98	1	7	0.83	0.51
13	1.07	0.99	1	7	0.84	0.53
16	1.31	1.09	1	7	0.75	0.42
16	1.31	1.09	1	8	0.77	0.49
16	1.30	1.09	1	9	0.75	0.41
16	1.30	1.09	1	8	0.74	0.42
16	1.31	1.10	1	7	0.77	0.45
16	1.31	1.09	1	8	0.75	0.40
39	3.19	1.68	3	13	0.46	0.12
39	3.20	1.69	3	13	0.48	0.17
39	3.19	1.69	3	14	0.47	0.18
39	3.18	1.69	3	13	0.47	0.19
39	3.18	1.68	3	13	0.46	0.15
39	3.18	1.69	3	12	0.47	0.16
76	6.22	2.32	6	18	0.32	0.03
76	6.21	2.32	6	17	0.32	0.07
76	6.21	2.31	6	19	0.33	0.08
76	6.20	2.33	6	17	0.31	0.05
76	6.21	2.32	6	18	0.32	0.06
76	6.21	2.31	6	18	0.31	0.03

[1] The statistical distributions of y (including mean, standard deviation, median, maximum value, skew, and kurtosis) for given x are obtained from 100,000 random samples and listed in the columns 2–7 of the table. Skew is defined by the ratio of the third-order moment to (standard deviation)^3. Kurtosis is defined by the ratio of the fourth-order moment to (variance)^2 minus 3.

treated y as a fluctuating quantity in each group of given x, calculating the statistical distribution of y. The resulting distributions are presented in Table 2.

Upon examining Table 2, we observe that the mean value of y remains constant within each group, specifically y=$(a/1273)x$, where a represents the number of sites in set A(a = 104). This constancy arises from the fact that the probability of a stochastic-produced site occurring in set A is $a/1273$, and the total occurrence is given by $(a/1273)x$ for x sites. Additionally, the skew value remains approximately constant for a given x and decreases as x increases. Consequently, the parameter y tends towards a normal distribution as x becomes larger. It is worth noting that extending the randomization of y from six times to a greater number of times does not alter the aforementioned conclusion. Thus, randomizing y for a given x to expand the range of stochastic sampling is a viable approach. This technique effectively increases stochastic information and demonstrates the reliability of the stochastic method in the A-X model.

3.5. The prediction of macro-lineage of SARS-CoV-2

By employing the A-X model, we can make predictions regarding the emergence of a new macro-lineage P, along with the already known macro-lineages N and O, when the number of sites (x) in X is sufficiently large. In Fig. 4, we have illustrated how this new macro-lineage can arise through stochastic sampling under the condition of large x. To further investigate this phenomenon, let us consider the following example: a = 104 for set A, x = 77 and y = 6 for set X. The resulting UPGMA tree is presented in Fig. 5. Our analysis reveals that the newly identified strain, New77.6, is not classified under macro-lineages N or O, but instead falls into a distinct macro-lineage, P. The results consistently hold true across various sample sets and randomizations, indicating the inevitable emergence of the novel macro-lineage P when x reaches a sufficiently large value.

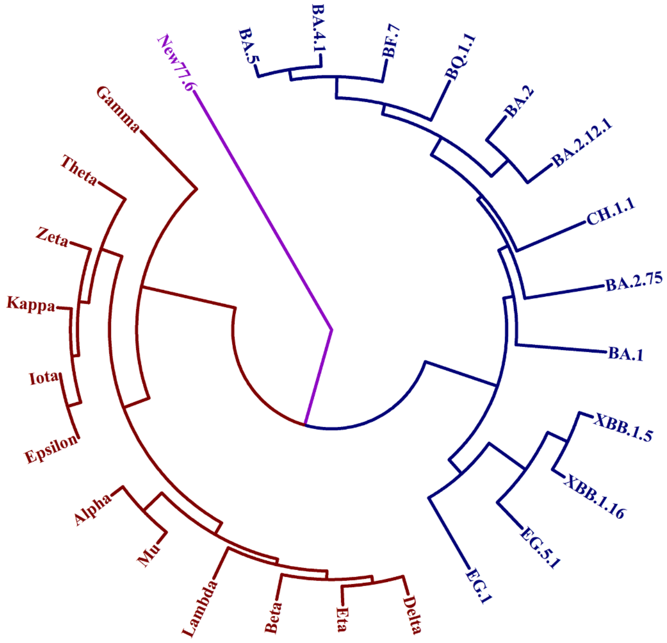

Fig. 5. The generation of new macro-lineage P – an example.

Another issue arises concerning the appearance of the new macro-lineage P, which is dependent upon the number 'a ' of sites within set A. In the aforementioned discussion, a value of a = 104 is assumed based on data from 25 mutants sourced from outbreak.info (https://outbreak.info/, accessed on 15 October 2023). If two additional mutants, HV.1 and JN.1, are incorporated into set A, the value of a increases from 104 to 121. As a subset of variants has transitioned from set X to set A, the emergence of P is expected to be more rigorously constrained.

To delve into the formation of the new macro-lineage P, let us examine the generation of 10^4–10^5 new variants for each specific x value. The probability of the N, O, or P-lineage at a given x is determined by dividing its occurrence count by the total number of variants. The findings of part calculations are succinctly presented in Fig. 6, where the probability of the j-lineage (j = N, O, or P) is plotted against x. Fig. 6A is plotted for 25 mutants (a = 104) and Fig. 6B for 27 mutants (a = 121).

In our A-X model, the selection of set X is stochastic, resulting in the stochastic occurrence of new variants on the tree. Nonetheless, we have demonstrated that the generation of multiple macro-lineages and the subsequent tree topology bifurcation into several major branches are both certain and unavoidable. Furthermore, we have proved that the assignment of a macro-lineage to a new variant is statistically dependent on x, and there are specific demarcation values of x that differentiate between different macro-lineages. The demarcation values of x provide a more detailed classification of the occurrence of the three macro-lineages. By performing 10^4–10^5 iterations of stochastic production of the x-long sequence and randomizing the parameter y several times, we discovered that the demarcation values of x are as follows:

New$x.y$∈N when $x \le 13$; New$x.y$∈N or O when $13 < x \le 16$; New$x.y$∈N or O or P when $16 < x \le 39$; New$x.y$∈O or P when $39 < x \le 76$; and New$x.y$∈P when $x > 76$. (in Fig. 6A);

New$x.y$∈N when $x \le 16$; New$x.y$∈N or O when $16 < x \le 21$; New$x.y$∈N or O or P when $21 < x \le 38$; New$x.y$∈O or P when $38 < x \le 110$; and New$x.y$∈P when $x > 110$. (in Fig. 6B)

By comparing Fig. 6B with Fig. 6A, one can discern the developmental trend of virus mutation. Two possibilities arise. The first involves the continuous expansion of set A, which includes only two older macro-lineages, N and O, with the demarcation values of x (i.e., x_{dem}) steadily increasing. The second possibility is that both the halt in increases in the total number 'a' of sites within set A and in the demarcation value x_{dem} occurred at a specific point in time. In the latter case, the new macro-

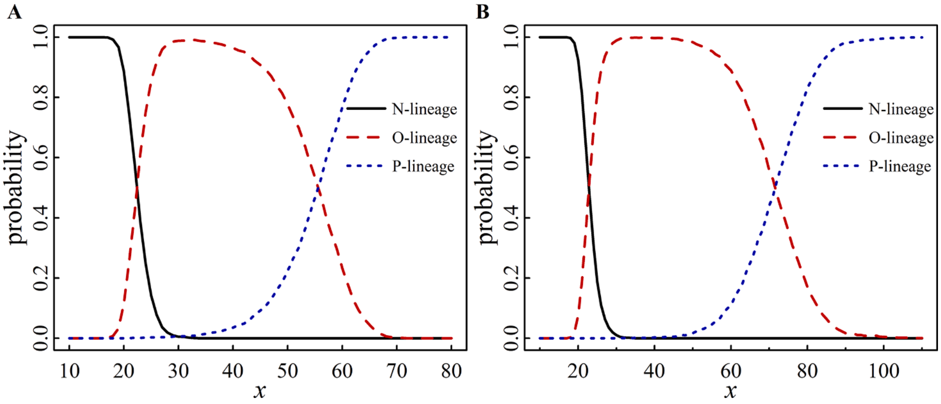

Fig. 6. The generation of three macro-lineages with respect to parameter *x*. The probability of the N-, O- or P-lineage is plotted against *x*. (A) is plotted for 25 mutants ($a = 104$) and (B) for 27 mutants ($a = 121$).

Table 3
Electric charge dependence of virus mutation[1].

Macro-lineages	Mutant	Number of AA sites	Positively charged	Negatively charged	Neutrally charged
N-lineage	Lambda	14	3	1	10
	Gamma	12	3	5	6
	Beta	10	5	2	4
	Alpha	10	5	3	3
	Mu	9	7	1	2
	Eta	9	6	1	3
	Delta	9	7	1	1
	Theta	7	6	3	1
	Kappa	5	5	0	0
	Iota	4	2	0	2
	Epsilon	4	2	0	2
	Zeta	3	3	0	1
O-lineage	BA.1	33	16	6	13
	BA.5	34	14	8	14

[1] The basic residue is assigned a charge of +1, the acidic residue a charge of −1, and all others are assigned a charge of 0. The increase in charge is determined by the algebraic difference between the mutated residue and the wild type. The positive (negative) values in the table represent the sum of charge increases for residues with positive (negative) charge. The neutral values in the table correspond to the total number of residues with no change in charge.

lineage P would emerge after x surpasses x_{dem}. In the context of SARS-CoV-2 mutation history, we observed the emergence of the new Omicron lineage in winter 2021, along with a sudden cessation in the increase of total mutational sites within the old N lineage ($a \leq 58$) at the beginning of 2021. This observation indicates the occurrence of the second possibility in history. It is essential to monitor the potential emergence of the P lineage in the future.

4. Discussions

4.1. On mutational robustness

A genotype is denoted by a four-letter (or two-letter) sequence, where a mutant can be considered a variant of the genotype. The evolutionary relationship among a collection of mutants, depicted as an evolutionary tree, is referred to as the evolutionary phenotype. Furthermore, distinct boundaries are observed between any pair of macro-lineages within the evolutionary tree, indicating a pronounced phenotype bias that shows the robustness in the genotype-phenotype mapping. Each group of mutants is assigned to a specific branch on the evolutionary tree, such as the alpha-beta-gamma-delta branch (macro-lineage N) or the omicron branch (macro-lineage O), among others. The origin of the phenotype robustness stems from the effective structuring among diverse genotypes. Notably, the interconnection between different macro-lineages is sustained by the high mutational robustness present in the system. We observed that the number of mutated sites in the sequence plays a crucial factor in the connection. Mutants in the N branch exhibit 58 mutated sites, whereas those in the O branch have more than 87 sites. The evolution from an earlier branch to a later branch occurs through an increase in the number of mutated sites. Our calculations indicated that when the number of mutated sites is sufficiently large, there is a nonzero probability of generating a new macro-lineage (macro-branch P on the tree). Thus, the evolutionary theoretical study provides evidence for the presence of mutational robustness in virus evolution. The concept of robustness in the genotype-phenotype map and the mutational robustness were proposed in (Wagner, 2007; Ahnert, 2017; Mohanty et al., 2023). Our study provides an additional example of mutational robustness in virus evolution.

4.2. Electric charge dependence of virus mutation

Apart from immune evasion, it is generally believed that the primary force driving virus mutation is intrinsic transmissibility, which is mainly determined by the ACE2 binding affinity. However, the ACE2 binding affinity only affects the receptor-binding domain (RBD). Are there any other physical forces that influence the entire spike protein domain? The literature has highlighted the significant role of electrostatic interaction in biological systems (Zhou and Pang, 2018). The population of conformational states can be determined by examining the free energy change during conformational transitions of the spike protein. Electrostatic interaction plays a crucial role in determining this free energy change (Luo and Lv, 2023). As commonly known, the twenty amino acids (AAs) can be classified into three types: D, E, and Y are acidic residues (negatively charged), H, K, and R are basic residues (positively charged), and the remaining amino acids are classified as neutral residues. The viewpoint presented above regarding the relationship between conformational change and electrostatic interaction suggests that variations in amino acid charge may potentially trigger mutations in the spike structure. Therefore, changes in amino acid charge represent structural potential in virus mutations, similar to the ACE2 binding affinity but affecting the entire spike protein. To evaluate the influence of electric charge on virus mutation, we calculated and presented the results in Table 3 (only two mutants for omicron are listed since the cases for other mutants in macro-lineage O are similar).

Analysis of Table 3 reveals that, for the majority of mutants, there is a tendency towards a positive charge in the alteration of amino acid charge during mutation. Previous works (Cotton et al., 2023; Pawłowski, 2021) indicate that positively charged amino acid types are generally observed during mutations. However, our calculations indicate that this trend is more pronounced in macro-lineages O. In macro-lineages N, the trend is less apparent, and there are counterexamples. The fundamental principle of virus mutation is the presence of electric charge dependence, which exhibits distinct characteristics in different lineages and macro-lineages (Božič and Podgornik, 2023).

4.3. *Conclusions drawn from the current study*

1. We propose representing the SARS-CoV-2 virus strain with a 4-letter sequence, based on amino acid mutations within the spike protein.
2. The application of an *n*-distance algorithm in UPGMA effectively yields a variant phylogenetic tree that closely aligns with experimental data on virus evolution.
3. We introduce the A-X model for generating new strains on the phylogenetic tree. By combining set A (comprising existing mutated sites) and set X (including x randomly generated sites), detailed studies on the emergence of new strains can be conducted.
4. Expanding the scope of stochastic sampling can be achieved through two means: increasing the size of x and randomizing the parameter y within the intersection set $Y = A \cap X$.
5. When x reaches a sufficient scale, a new macro-lineage of SARS-CoV-2 is predicted, alongside existing lineages. We have derived demarcation values of x that differentiate between various macro-lineages.
6. Therefore, we have proposed a logically simple theory of virus mutation to enhance our understanding of the evolution of SARS-CoV-2.

Funding

This research did not receive any specific grant from funding agencies in the public, commercial, or not-for-profit sectors.

Author statement

We, the authors of the manuscript titled “An evolutionary theory on virus mutation in COVID-19”, declare that the data, methods, and conclusions presented in our submission to Virus Research have not been published in any peer-reviewed journal. The content of the paper does not involve any ethical or moral issues. Furthermore, there are no conflicts of interest among the authors."

CRediT authorship contribution statement

Liaofu Luo: Conceptualization, Methodology, Investigation, Writing – original draft, Writing – review & editing. **Jun Lv:** Methodology, Validation, Data curation, Investigation, Visualization, Writing – original draft, Writing – review & editing.

Declaration of competing interest

The authors declare that they have no known competing financial interests or personal relationships that could have appeared to influence the work reported in this paper.

Data availability

No data was used for the research described in the article.

Acknowledgments

We express our gratitude to Dr Ying Zhang for her assistance with data collection, valuable discussions, and insightful suggestions. We also acknowledge the data on 25 SARS-CoV-2 variants obtained from outbreak.info.

References

Ahnert, S.E., 2017. Structural properties of genotype-phenotype maps. J. R. Soc. Interface 14, 20170275. https://doi.org/10.1098/rsif.2017.0275.

Božič, A., Podgornik, R., 2023. Evolutionary changes in the number of dissociable amino acids on spike proteins and nucleoproteins of SARS-CoV-2 variants. Virus. Evol. 9, vead040. https://doi.org/10.1093/ve/vead040.

Callaway, E., 2021. Beyond Omicron: what’s next for COVID’s viral evolution. Nature 600, 204–207. https://doi.org/10.1038/d41586-021-03619-8.

Cao, Y., Jian, F., Wang, J., Yu, Y., Song, W., Yisimayi, A., Wang, J., An, R., Chen, X., Zhang, N., Wang, Y., Wang, P., Zhao, L., Sun, H., Yu, L., Yang, S., Niu, X., Xiao, T., Gu, Q., Shao, F., Hao, X., Xu, Y., Jin, R., Shen, Z., Wang, Y., Xie, X.S., 2023. Imprinted SARS-CoV-2 humoral immunity induces convergent Omicron RBD evolution. Nature 614, 521–529. https://doi.org/10.1038/s41586-022-05644-7.

Carabelli, A.M., Peacock, T.P., Thorne, L.G., Harvey, W.T., Hughes, J., , COVID-19 Genomics UK Consortium, Peacock, S.J., Barclay, W.S., de Silva, T.I., Towers, G.J., Robertson, D.L., 2023. SARS-CoV-2 variant biology: immune escape, transmission and fitness. Nat. Rev. Microbiol. 21, 162–177. https://doi.org/10.1038/s41579-022-00841-7.

Cotten, M., Phan, M.V.T., 2023. Evolution of increased positive charge on the SARS-CoV-2 spike protein may be adaptation to human transmission. iScience 26, 106230. https://doi.org/10.1016/j.isci.2023.106230.

Elnaggar, A., Heinzinger, M., Dallago, C., Rehawi, G., Wang, Y., Jones, L., Gibbs, T., Feher, T., Angerer, C., Steinegger, M., Bhowmik, D., Rost, B., 2022. ProtTrans: toward understanding the language of life through self-supervised learning. IEEE Trans. Pattern Anal. Mach. Intell. 44, 7112–7127. https://doi.org/10.1109/TPAMI.2021.3095381.

Ferruz, N., Schmidt, S., Höcker, B., 2022. ProtGPT2 is a deep unsupervised language model for protein design. Nat. Commun. 13, 4348. https://doi.org/10.1038/s41467-022-32007-7.

Fowler, D., Fields, S., 2014. Deep mutational scanning: a new style of protein science. Nat. Methods 11, 801–807. https://doi.org/10.1038/nmeth.3027.

Gangavarapu, K., Latif, A.A., Mullen, J.L., Alkuzweny, M., Hufbauer, E., Tsueng, G., Haag, E., Zeller, M., Aceves, C.M., Zaiets, K., Cano, M., Zhou, X., Qian, Z., Sattler, R., Matteson, N.L., Levy, J.I., Lee, R.T.C., Freitas, L., Maurer-Stroh, S., , GISAID Core and Curation Team, Suchard, M.A., Wu, C., Su, A.I., Andersen, K.G., Hughes, L.D., 2023. Outbreak.info genomic reports: scalable and dynamic surveillance of SARS-CoV-2 variants and mutations. Nat. Methods 20, 512–522. https://doi.org/10.1038/s41592-023-01769-3.

Li, W.H., 1997. Molecular Evolution. Sinauer Associates Inc., Sunderland, MA.

Luo, L., Lv, J., 2023. Mathematical modelling of virus spreading in COVID-19. Viruses 15, 1788. https://doi.org/10.3390/v15091788.

Ma, W., Fu, H., Jian, F., Cao, Y., Li, M., 2023. Immune evasion and ACE2 binding affinity contribute to SARS-CoV-2 evolution. Nat. Ecol. Evol. 7, 1457–1466. https://doi.org/10.1038/s41559-023-02123-8.

Mallapaty, S., 2022. Where did Omicron come from? Three key theories. Nature 602, 26–28. https://doi.org/10.1038/d41586-022-00215-2.

Markov, P.V., Ghafari, M., Beer, M., Lythgoe, K., Simmonds, P., Stilianakis, N.I., Katzourakis, A., 2023. The evolution of SARS-CoV-2. Nat. Rev. Microbiol. 21, 361–379. https://doi.org/10.1038/s41579-023-00878-2.

Mohanty, V., Greenbury, S.F., Sarkany, T., Narayanan, S., Dingle, K., Ahnert, S.E., Louis, A.A., 2023. Maximum mutational robustness in genotype-phenotype maps follows a self-similar blancmange-like curve. J. R. Soc. Interface 20, 20230169. https://doi.org/10.1098/rsif.2023.0169.

Nei, M., Kumar, S., 2000. Molecular Evolution and Phylogenetics. Oxford University Press, New York.

Pawłowski, P.H., 2021. Additional positive electric residues in the crucial spike glycoprotein S regions of the new SARS-CoV-2 variants. Infect. Drug Resist. 14, 5099–5105. https://doi.org/10.2147/IDR.S342068.

Rahnsch, B., Taghizadeh, L., 2024. Network-based uncertainty quantification for mathematical models in epidemiology. J. Theor. Biol. 577, 111671 https://doi.org/10.1016/j.jtbi.2023.111671.

Ramachandran, A., Lumetta, S.S., Chen, D., 2024. PandoGen: generating complete instances of future SARS-CoV-2 sequences using deep learning. PLoS Comput. Biol. 20, e1011790 https://doi.org/10.1371/journal.pcbi.1011790.

Starr, T.N., Greaney, A.J., Hilton, S.K., Ellis, D., Crawford, K.H.D., Dingens, A.S., Navarro, M.J., Bowen, J.E., Tortorici, M.A., Walls, A.C., King, N.P., Veesler, D., Bloom, J.D., 2020. Deep mutational scanning of SARS-CoV-2 receptor binding domain reveals constraints on folding and ACE2 binding. Cell 182, 1295–1310. https://doi.org/10.1016/j.cell.2020.08.012. .e20.

Wagner, A., 2007. Robustness and Evolvability in Living Systems. Princeton University Press, New York.

Wang, Q., Iketani, S., Li, Z., Liu, L., Guo, Y., Huang, Y., Bowen, A.D., Liu, M., Wang, M., Yu, J., Valdez, R., Lauring, A.S., Sheng, Z., Wang, H.H., Gordon, A., Liu, L., Ho, D.D., 2023. Alarming antibody evasion properties of rising SARS-CoV-2 BQ and XBB subvariants. Cell 186, 279–286. https://doi.org/10.1016/j.cell.2022.12.018. .e8.

Zhou, H.X., Pang, X., 2018. Electrostatic interactions in protein structure, folding, binding, and condensation. Chem. Rev. 118, 1691–1741. https://doi.org/10.1021/acs.chemrev.7b00305.